Conductance measurements of polar molecules in a non-conducting solvent†

Clark Otey,⊥ Mukund Sharma,⊥ Jazmine Prana, Thomas M. Czyszczon-Burton, Alejandro Hernandez, and Michael S. Inkpen*

Department of Chemistry, University of Southern California, Los Angeles, CA 90089, USA. E-mail: inkpen@usc.edu.

† Supplementary Information available: Additional experimental details, conductance and computational data.

⊥ C.O. and M.S. contributed equally to this work.

Solution-based single-molecule conductance measurements of *α*,ω-bis(carboxylic acids) are conveniently performed using high-boiling point, non-conducting ethereal solvents. Tunnel coupling calculations support experimental observations that linear oligoalkanes exhibit the expected exponential decay of conductance with length, whereas junctions comprising cyclic bridge hydrocarbons of different length and/or structure exhibit a similar conductance.

A central goal of molecular electronics is to develop functional molecular-scale components that may one day serve as nanoscale electronic circuit elements.[1] To drive advances, a deeper understanding of the complex interplay between electrode, linker group, and molecular backbone properties, and the impact on charge transport through metal-molecule-metal junctions, is required. We focus here on carboxylic acids, well-recognized electrode linkers that facilitate the spontaneous formation of single-molecule junctions from aqueous solutions[2,3] or components adsorbed/deposited on surfaces (**Fig. 1a**).[4,5] Their weak acid character, hydrophilicity, and reactivity have enabled studies exploring the pH-dependence of junction conductance,[3,5,6] the use of electrochemically-stabilized silver, copper, and palladium metal electrodes,[7–9] or the reversible formation of ester-containing molecular circuits.[4] However, the capacity of bis(carboxylic acids) to generate extended hydrogen-bonding networks in the solid state[10] can limit their solubility in commonly used, electrically-insulating, scanning tunnelling microscope (STM) solvents. To date, only two single-molecule conductance studies in such solvents have been reported: one using tetradecane (TD), restricted to compounds comprising a *single* carboxylic acid,[6] and one of bis(carboxylic acids) in toluene.[7]

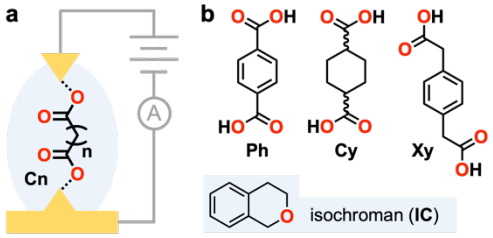

Figure 1. (a) A schematic of molecular junctions formed from linear oligoalkane *α*,ω-bis(carboxylic acids) (**Cn**, n = 2, 4, 6, 8) bound between gold electrodes. **(b)** Molecular structures of cyclic *α*,ω-bis(carboxylic acid) junction components (**Ph**, **Cy**, **Xy**) and the high boiling point ethereal solvent isochroman (**IC**).

In this work we report that non-conducting organic solvents comprising oxygen functionalities (hard donors) improve the solubility of bis(carboxylic acids) of interest, presumably by disrupting analyte-analyte intermolecular interactions. Critically, the use of isochroman (**IC**; **Fig. 1b**), enables conductance measurements of polar *α*,ω-bis(carboxylic acids) with different backbones using uncoated STM tips. These experimental studies, supported by electronic structure calculations of model junctions, provide important new insights into the nature of charge transport across the -AuOC(O)- interfacial contact.

We perform single-molecule conductance measurements using the STM-based break junction (STM-BJ) method (see the **SI** for more details).[11,12] This technique involves repeatedly pushing an uncoated gold tip in and out of a gold substrate while applying a voltage bias (V_{bias}) between these electrodes and measuring the current (I) as a function of tip-substrate displacement. Step features observed in the resulting conductance ($G = I/V_{bias}$)-displacement traces correspond to the formation of Au-Au point contacts at integer multiples of 1 G_0 (= $2e^2/h$), and molecular junctions at lower conductance (after addition of an analyte in solution). Thousands of these conductance traces are compiled, without data-selection, into 1D conductance and 2D conductance-displacement histograms. The resulting histogram features reveal the

most probable properties (conductance, maximum displacement) of the junctions studied (**Fig. 1a**).

The utility of four different high-boiling point (BP) ethereal solvents for STM-BJ studies was first evaluated using 4,4'-bipyridine (**bipy**). Two solvents are cyclic ethers: isochroman (**IC**; BP ~ 214°C) and 2,3-dihydrobenzofuran (**DHBF**; 188°C). The other two are acyclic ethers: dioctylether (**DOE**; 286°C) and cyclopentyl methyl ether (**CPME**; 106°C). Explicit molecular structures for these compounds are provided in **Fig. S1a**. From each measurement we obtain histograms comprising the characteristic two peak feature of **bipy** junctions, corresponding to N lone pair-Au and pyridyl π-Au contact geometries,[13] confirming these solvents do not impede junction formation (**Fig. S1b-e**). The conductance of junctions measured in these solvents typically lie between or above those obtained from measurements in TD or 1,2,4-trichlorobenzene (TCB), further indicating these new solvents only weakly interact with the gold surface (**Table S1**).[14,15] We note that, due to the relatively low boiling point of **CPME**, additional drops of pure solvent must be added during experiments to compensate for evaporative losses. The low instrument noise floor observed in these, and subsequent, histograms illustrate the electrically insulating nature of these solvents. We select **IC** for additional STM-BJ studies given its moderate boiling point and mixed aliphatic-aromatic structure which we reason will help solubilize a wider range of compounds.

We subsequently perform conductance measurements using **IC** solutions of alkane α,ω-bis(carboxylic acids) (**Cn**, where n is the number of carbon atoms between HOC(O)- linkers; **Fig. 1a**). Specifically, we study butanedioic (**C2**), hexanedioic (**C4**), octanedioic (**C6**), and decanedioic (**C8**) acid. We plot, in **Fig. 2**, overlaid 1D histograms for these diacids. All histograms comprise a sharp peak feature towards lower conductance, assigned to single-molecule junctions. In each case we also observe an additional peak or shoulder at ~2× the conductance of the first peak, which we attribute to the formation of junctions with two molecules in parallel. These distinct features are also clearly observed in the corresponding 2D histograms, as illustrated in **Fig. 2b** for **C6**. A semilog plot of the most probable conductance for each single-molecule junction against n shows these values exhibit an exponential length dependence indicative of tunnelling transport (**Fig. 2**-*inset*). We obtain a tunnelling decay constant, β, of 0.90/n and a contact conductance, G_c, of 7.2×10^{-3} G_0 from a linear fit to this data using $G = G_c \cdot \exp(-\beta n)$. This β is consistent with values obtained for other series of oligoalkanes with different linker groups, and the low G_c (e.g., relative to 4.8×10^{-2} G_0 for -SMe), attributed to the additional carbon atom in the linker group, also agree well with previous reports.[3,6,7,16] Conductance data for all diacid junctions is provided in **Table S2**.

While solutions of ethanedioic acid (**C0**) can also be prepared in **IC** (at least to ~0.5 mM), no clear junction features are observed in STM-BJ studies. We attribute this to the short length of **C0**, which will provide only small step features in conductance traces and could also reduce the probability of molecular junction formation.[6] Analysis of 2D histograms reveals that the maximum displacement of **Cn** junctions decreases by 1-2 Å as n is reduced

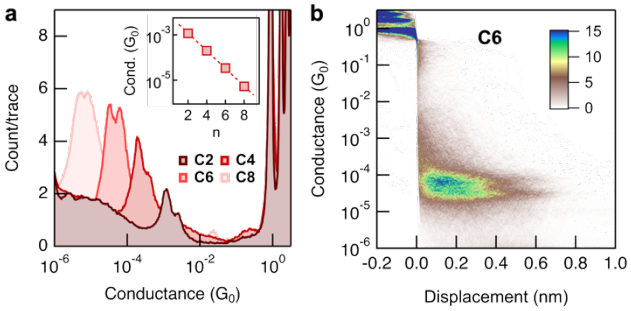

Figure 2. (a) Overlaid 1D histograms for **Cn** measured in **IC** (V_{bias} = 250 mV, 5,000 traces). *Inset:* a plot of the experimental single-molecule conductance against n (β = 0.90/n). **(b)** 2D histogram for **C6**.

by 2, and that **C2** junctions typically extend to a displacement of ~2 Å (**Fig. 2b** and **S2**). Notably, this result contrasts with previous studies, for example, on silver and copper electrodes, which have observed conductance features in measurements of **C0**.[17] For completeness, we report that a conductance peak for **C6** can be obtained from an analyte-coated substrate after drop casting a ~20 mM solution in THF (**Fig. S4**). However, we find this method of introducing junction components to be less consistent than solution studies which provide greater control over the local concentration of analyte molecules near the junction. Notably, conductance studies of **C6** as a saturated solution in TCB provided only broad, ill-defined conductance features, further highlighting the utility of **IC** for STM-BJ measurements of polar analytes.

We next evaluate the conductance of junctions formed from α,ω-bis(carboxylic acids) comprising cyclic 1,4-phenylene (**Ph**, n = 4; benzene-1,4-dicarboxylic acid), 1,4-cyclohexane (**Cy**, n = 4; 1,4-cyclohexanedicarboxylic acid), and 1,4-xylylene (**Xy**, n = 6; *p*-phenylenediacetic acid) backbones (for molecular structures, see **Fig. 1b**). Here, values of n indicate the number of carbon atoms linked through a single branch of the backbone ring. We plot, in **Fig. 3a**, overlaid 1D conductance histograms for these cyclic diacids, in which we again typically observe two overlapping peaks that indicate the formation of one and two molecular junctions. Remarkably, while their hydrocarbon bridges differ in the number and structure (aliphatic, aromatic) of carbon atoms, their junctions each exhibit a conductance within a factor of ×1.1 from each other and between 60-68% of the conductance of **C4** (**Table S2**). Repeated

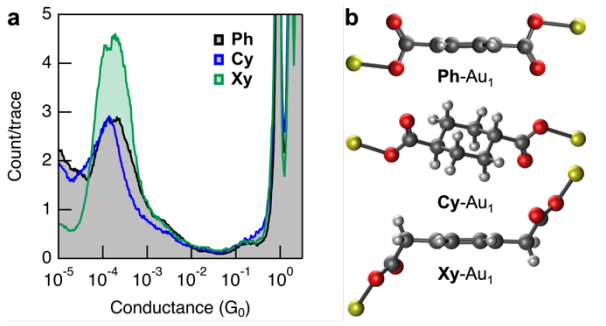

Figure 3. (a) Overlaid 1D histograms for measurements of **Ph** (black), **Cy** (green), and **Xy** (blue) in **IC** (V_{bias} = 250 mV, 5,000-10,000 traces). **(b)** Au_1-cluster junction geometries (orthographic view) that provide the highest calculated tunnel couplings for each cyclic molecular backbone.

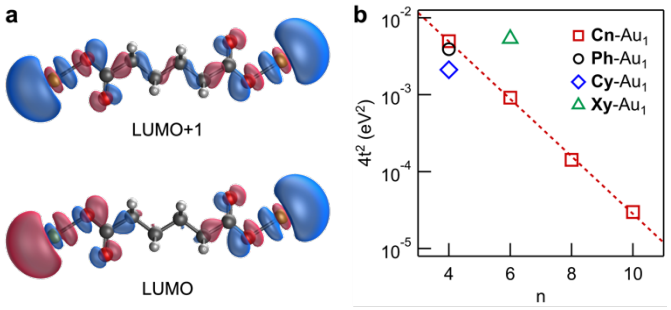

Figure 4. (a) Isosurface plots (isovalue = 0.06 Å^{-3}) of the DFT-calculated, tunnel coupled, LUMO and LUMO+1 orbitals for **C4**-Au$_1$. **(b)** A plot of the calculated tunnel couplings for **Cn**-Au$_1$ (squares) against n (β = 0.86/n), overlaid with the largest tunnel coupling for **Ph**-Au$_1$ (circle), **Cy**-Au$_1$ (diamond), and **Xy**-Au$_1$ (triangle).

measurements of these analytes highlight the reproducibility of this result (**Fig. S3a-c**). Our findings contrast with the ~10× higher conductance reported for **Ph** compared to **Xy** junctions formed using copper electrodes,[18] although the conductance data obtained for **Ph** in that study included additional peak features at lower conductance.

To provide additional insights into the electronic properties of these carboxylic acid-linked junctions, we undertake first principles calculations based on density functional theory (DFT; detailed methods are provided in the **SI**). Briefly here, we replace the protons of each carboxylic acid linker with a single gold atom to form Au$_1$ cluster junctions. Each contact is modelled using a κ^1 (O-monodentate) coordination mode, noting that this geometry is observed in molecular structures of Au(I)-carboxylate complexes determined from single-crystal X-ray diffraction.[19] Given that rotations about the unconstrained and sterically unimpeded single bonds in each system (e.g., AuOC(O)-aryl) are expected to be soft degrees of freedom,[14,20] we perform geometry optimizations of each junction using input structures with different dihedral angles (**Fig. S5**).

In **Fig. 3b** we plot illustrative optimized geometries for **Ph**-Au$_1$, **Cy**-Au$_1$, and **Xy**-Au$_1$ which support a qualitative rationalization of the measured conductance for these junctions. For **Cy**, transport is through a *sp*^{3}-hybridized n = 4 backbone, providing a similar, but lower conductance to **C4**. This conductance ordering may be rationalized given that the structural constraints of the cyclohexane group ensure the alkane chain between each linker cannot adopt a more conductive all-*trans* configuration;[21] yet it is also possible that transmission through this cyclic hydrocarbon backbone is reduced through destructive quantum interference effects.[22] While transport through conjugated phenylene backbones may be expected to be more efficient than through non-conjugated alkanes, we note that the geometry of the carboxylic acid linker in **Ph** orients the Au-O bond in the plane of the benzene ring. This minimizes electronic coupling between the electrode and the π-system, forcing charge transport through the *sp*^{2}-hybridized C-C framework. A similar rationale has been applied to justify the lower conductance of Au-1,4-phenylene-Au versus Au-(CH$_2$)$_4$-Au junctions.[23] Finally, for **Xy** it is possible to access junction geometries that better align the terminal AuOC(O)- groups with the conjugated phenylene backbone, apparently providing a comparable junction conductance to **Ph** and **Cy** despite the longer, n = 6, conduction path.

To further interrogate the conductance trends observed for linear and cyclic diacid junctions we apply these and additional Au$_1$ cluster models to calculate tunnel couplings for each system (4t^2). These values have previously been found to correlate well with the experimental conductance of junctions comprising neutral linker groups (-NH$_2$, -PR$_2$, -SMe) with different bridges.[24,25] In the present study, however, we utilize a negatively charged carboxylate linker, effectively replacing 2×H$^+$ with 2×Au$^+$ in each Au$_1$ cluster model to provide a charge neutral closed shell system. We therefore probe carboxylate-linked models with 2 fewer electrons than found in analogous systems with neutral linkers (which add 2×Au atoms). The relevant pair of orbitals, tunnel coupled through the molecular backbone with energy splitting of 2t, are therefore LUMO and LUMO+1 rather than HOMO and LUMO. As shown in **Fig, 4a** for **C4**-Au$_1$, these form a symmetric and antisymmetric pair exhibiting Au *s*-O *p* antibonding character (analogous orbital pairs are provided for other junction models in **Fig. S7**).

We validate our approach by plotting, in **Fig. 4b**, 4t^2 versus n for **Cn**-Au$_1$ models (n = 4-10). From a linear fit to these data, substituting G = 4t^2 into G = G$_c$·exp(−βn), we obtain β = 0.86/n, in good agreement with our experimental result (**Fig. 2a**). In **Fig. 4b**, we also overlay the largest tunnel couplings obtained from all the optimized geometries so far evaluated for **Ph**-Au$_1$, **Cy**-Au$_1$, and **Xy**-Au$_1$ junctions (these couplings are calculated for the geometries shown in **Fig. 3b**). While the tunnel coupling for each junction component is clearly dependent on the precise conformation of the junction model (**Table S4**), the similarity of each of these maximum couplings to each other, and to the tunnel coupling obtained for **C4**-Au$_1$, supports our experimental finding that junctions formed from this series of molecules can exhibit a similar conductance. To evaluate the relative probabilities, and thermal population, of each conformation during STM-BJ studies, the potential energy landscapes of these junctions could be explored in future studies.

While our calculations are self-consistent, we stress that the coordination mode of carboxylic acids to gold or other metal nanoelectrodes may not always be κ^1. Indeed, molecular structures of Ag(I) and Cu(I) complexes determined by single-crystal X-ray diffraction provide several examples of κ^2 (O,O-bidentate) or bridging coordination geometries.[19] Fortunately this linker characteristic may not prove critical to the interpretation of conductance data, transmission calculations by Huang *et al.* suggest that the binding of -COO$^-$ to gold through either κ^1 or κ^2 coordination modes does not strongly affect junction conductance.[2] Though the precise coordination mode may vary, these linker groups are considered to bind in junctions as carboxylates (-COO$^-$). No conductance features are observed in studies of analytes with carboxylic acid methyl ester terminations (and in some studies at low pH).[3,6] Recent DFT calculations of phenol and phenolate linkers also indicate that Au-O binding is more energetically favourable after deprotonation,[26] arguably due to the increased basicity of RO$^-$ relative to ROH. We note that the apparent spontaneous deprotonation of a carboxylic acid upon

binding to gold is a process also considered critical for thiol[27] and terminal alkyne[28] groups. Interestingly, the much larger pK_a of the alkyne C–H group may implicate a distinct deprotonation mechanism (pK_a^{DMSO}: $PhCO_2H$ = 11.1, PhSH = 10.31, PhCCH = 28.7).[29]

Inspired by the plausible κ^1-binding of carboxylates to gold in single-molecule junctions, we propose that a carboxylic acid could be considered simply as an alcohol (-OH) linker comprising an acidic proton; the negative charge of the conjugate base stabilized by resonance with the adjacent carbonyl group. While -OH groups have to date scarcely been explored as linkers in single-molecule electronics, we propose they may be more widely utilized after deprotonation through addition of a sufficiently strong base (as recently reported for phenol),[26] or after spontaneous deprotonation at a metal interface through the incorporation of appropriate adjacent chemical functionality that lowers their pK_a. Such contact chemistries could prove useful for forming junctions with oxophilic metal electrodes, or to evaluate *in situ* chemical reactions thought to result in alkoxide-terminated junctions.[30]

Taken together, the results of this study motivate additional investigations using **IC** or related non-conductive ethereal solvents to probe the properties of carboxylic acid-linked single-molecule junctions. Our approach may be expanded to characterize other families of compounds with polar backbones or distinct contact groups, such as amino acids or species with charged/ionic character such as deprotonated alcohols.[26] More broadly, we recognize that by substituting polar solvents such as water or propylene carbonate with non-conducting analogues that can perform a similar solubilizing function, we greatly simplify STM-BJ experiments that may otherwise require coated STM tips to minimize background electrochemical currents.[31] This is particularly relevant for glovebox-based STM-BJ methods – of increasing utility for the study of air-sensitive electrode metals[30] and molecules[32] – in which water must be strictly excluded and the frequent use of coated STM tips would likely present a substantial experimental burden.

Acknowledgments

This work was primarily supported by University of Southern California (USC) startup funds and the National Science Foundation (NSF CAREER Award to M.S.I., CHE2239614). A.H. thanks the NSF CAREER program, Agilent Technologies, and Steve and Cathy Gagliardi for their support of the USC-Cerritos Summer Internship in Sustainability program.

Conflicts of interest

There are no conflicts to declare.

Data availability

The data supporting this article have been included as part of the Supplementary Information.

References

1 T. A. Su, M. Neupane, M. L. Steigerwald, L. Venkataraman and C. Nuckolls, *Nature Reviews Materials*, 2016, **1**, 16002.
2 M. Huang, Q. Zhou, F. Liang, L. Yu, B. Xiao, Y. Li, M. Zhang, Y. Chen, J. He, S. Xiao and S. Chang, *Nano Lett.*, 2021, **21**, 5409–5414.
3 F. Chen, X. Li, J. Hihath, Z. Huang and N. J. Tao, *J. Am. Chem. Soc.*, 2006, **128**, 15874–15881.
4 M. S. Inkpen, Y. R. Leroux, P. Hapiot, L. M. Campos and L. Venkataraman, *Chemical Science*, 2017, **8**, 4340–4346.
5 S. Martín, W. Haiss, S. Higgins, P. Cea, M. C. López and R. J. Nichols, *J. Phys. Chem. C*, 2008, **112**, 3941–3948.
6 S. Ahn, S. V. Aradhya, R. S. Klausen, B. Capozzi, X. Roy, M. L. Steigerwald, C. Nuckolls and L. Venkataraman, *Physical Chemistry Chemical Physics*, 2012, **14**, 13841.
7 M.-W. Gu, H. H. Peng, I.-W. P. Chen and C. Chen, *Nat. Mater.*, 2021, **20**, 658–664.
8 X.-S. Zhou, J.-H. Liang, Z.-B. Chen and B.-W. Mao, *Electrochemistry Communications*, 2011, **13**, 407–410.
9 Y.-H. Wang, Z.-W. Hong, Y.-Y. Sun, D.-F. Li, D. Han, J.-F. Zheng, Z.-J. Niu and X.-S. Zhou, *J. Phys. Chem. C*, 2014, **118**, 18756–18761.
10 P. Li, M. R. Ryder and J. F. Stoddart, *Acc. Mater. Res.*, 2020, **1**, 77–87.
11 B. Xu and N. J. Tao, *Science*, 2003, **301**, 1221–1223.
12 L. Venkataraman, J. E. Klare, I. W. Tam, C. Nuckolls, M. S. Hybertsen and M. L. Steigerwald, *Nano Lett.*, 2006, **6**, 458–462.
13 S. Y. Quek, M. Kamenetska, M. L. Steigerwald, H. J. Choi, S. G. Louie, M. S. Hybertsen, J. B. Neaton and L. Venkataraman, *Nature Nanotechnology*, 2009, **4**, 230–234.
14 V. Fatemi, M. Kamenetska, J. B. Neaton and L. Venkataraman, *Nano Letters*, 2011, **11**, 1988–1992.
15 L. Kim, T. M. Czyszczon-Burton, K. M. Nguyen, S. Stukey, S. Lazar, J. Prana, Z. Miao, S. Park, S. F. Chen and M. S. Inkpen, *Nano Lett.*, 2024, **24**, 9998–10005.
16 Y. S. Park, A. C. Whalley, M. Kamenetska, M. L. Steigerwald, M. S. Hybertsen, C. Nuckolls and L. Venkataraman, *J. Am. Chem. Soc.*, 2007, **129**, 15768–15769.
17 Z.-L. Peng, Z.-B. Chen, X.-Y. Zhou, Y.-Y. Sun, J.-H. Liang, Z.-J. Niu, X.-S. Zhou and B.-W. Mao, *The Journal of Physical Chemistry C*, 2012, **116**, 21699–21705.
18 Z.-W. Hong, M. A. B. Aissa, L.-L. Peng, H. Xie, D.-L. Chen, J.-F. Zheng, Y. Shao, X.-S. Zhou, N. Raouafi and Z.-J. Niu, *Electrochemistry Communications*, 2016, **68**, 86–89.
19 A. Grodzicki, I. Łakomska, P. Piszczek, I. Szymańska and E. Szłyk, *Coordination Chemistry Reviews*, 2005, **249**, 2232–2258.
20 J. Prana, L. Kim, T. Czyszczon-Burton, G. Homann, S. Chen, Z. Miao, M. Camarasa-Gomez and M. Inkpen, *J. Am. Chem. Soc.*, 2024, **146**, 33265–33275.
21 D. R. Jones and A. Troisi, *J. Phys. Chem. C*, 2007, **111**, 14567–14573.
22 B. Zhang, M. H. Garner, L. Li, L. M. Campos, G. C. Solomon and L. Venkataraman, *Chemical Science*, 2021, **12**, 10299–10305.
23 Z. L. Cheng, R. Skouta, H. Vazquez, J. R. Widawsky, S. Schneebeli, W. Chen, M. S. Hybertsen, R. Breslow and L. Venkataraman, *Nat. Nanotechnol.*, 2011, **6**, 353–357.
24 A. Nitzan, *Annu. Rev. Phys. Chem.*, 2001, **52**, 681–750.
25 L. Venkataraman, J. E. Klare, C. Nuckolls, M. S. Hybertsen and M. L. Steigerwald, *Nature*, 2006, **442**, 904–907.
26 B. Lawson, H. E. Skipper and M. Kamenetska, *Nanoscale*, 2024, **16**, 2022–2029.
27 C. D. Bain, H. A. Biebuyck and G. M. Whitesides, *Langmuir*, 1989, **5**, 723–727.
28 D. Millar, L. Venkataraman and L. H. Doerrer, *J. Phys. Chem. C*, 2007, **111**, 17635–17639.
29 F. G. Bordwell, *Acc. Chem. Res.*, 1988, **21**, 456–463.
30 T. M. Czyszczon-Burton, E. Montes, J. Prana, S. Lazar, N. Rotthowe, S. F. Chen, H. Vázquez and M. S. Inkpen, *J. Am. Chem. Soc.*, 2024, **146**, 28516–28526.
31 L. A. Nagahara, T. Thundat and S. M. Lindsay, *Review of Scientific Instruments*, 1989, **60**, 3128–3130.
32 Z. Miao, T. Quainoo, T. M. Czyszczon-Burton, N. Rotthowe, J. M. Parr, Z. Liu and M. S. Inkpen, *Nano Lett.*, 2022, **22**, 8331–8338.